Aligned hemozoin crystals in curved clusters in malarial red blood cells revealed by nanoprobe X-ray Fe fluorescence and diffraction

Sergey Kapishnikov[a], Trine Berthing[b], Lars Hviid[c], Martin Dierolf[d,e], Andreas Menzel[d], Franz Pfeiffer[d,e], Jens Als-Nielsen[f,1], and Leslie Leiserowitz[a,1]

[a]Department of Materials and Interfaces, The Weizmann Institute of Science, Rehovot 76100, Israel; [b]Bionanotechnology and Nanomedicine, University of Copenhagen, 2100 Copenhagen, Denmark; [c]Center for Medical Parasitology, University of Copenhagen, 2100 Copenhagen, Denmark; [d]Paul Scherrer Institut, 5232 Villigen PSI, Switzerland; [e]Technische Universität München, 85748 Garching, Germany; and [f]Niels Bohr Institute, University of Copenhagen, 2100 Copenhagen, Denmark

Edited by* Ada Yonath, Weizmann Institue, Rehovot, Israel, and approved May 10, 2012 (received for review November 5, 2011)

The human malaria parasite *Plasmodium falciparum* detoxifies the heme byproduct of hemoglobin digestion in infected red blood cells by sequestration into submicron-sized hemozoin crystals. The crystal is composed of heme units interlinked to form cyclic dimers via reciprocal Fe—O (propionate) bonds. Templated hemozoin nucleation was envisaged to explain a classic observation by electron microscopy of a cluster of aligned hemozoin crystals within the parasite digestive vacuole. This dovetails with evidence that acylglycerol lipids are involved in hemozoin nucleation in vivo, and nucleation of β-hematin, the synthetic analogue of hemozoin, was consistently induced at an acylglycerol–water interface via their {100} crystal faces. In order to ascertain the nature of hemozoin nucleation in vivo, we probed the mutual orientations of hemozoin crystals in situ within RBCs using synchrotron-based X-ray nanoprobe Fe fluorescence and diffraction. The X-ray patterns indicated the presence of hemozoin clusters, each comprising several crystals aligned along their needle *c* axes and exposing {100} side faces to an approximately cylindrical surface, suggestive of nucleation via a common lipid layer. This experimental finding, and the associated nucleation model, are difficult to reconcile with recent reports of hemozoin formation within lipid droplets in the digestive vacuole. The diffraction results are verified by a study of the nucleation process using emerging tools of three-dimensional cellular microscopy, described in the companion paper.

crystal nucleation | optical birefringence | X-ray diffraction | submicrofocus X-ray fluorescence | lipid-induced precipitation

An early electron microscopy report by Goldberg et al. (1) described clusters of aligned hemozoin crystals within the digestive vacuole (DV) of *Plasmodium falciparum*. This raised the possibility of oriented nucleation, although the clustering and alignment might have occurred after the nucleation step. Fitch et al. (2) have proposed that neutral lipids play a role in inducing crystallization of hemozoin within the digestive vacuole (DV). The presence of lipid bodies a few hundred nm in diameter, composed of mono- and diacylglycerols close to the outer surface of the DV, has been reported by Jackson et al. (3). The authors postulated a role for these lipids in hemozoin precipitation, based on in vitro crystallization of synthetic hemozoin, namely β-hematin.

Many studies have demonstrated oriented nucleation of molecular crystals induced under crystalline monolayers of amphiphilic molecules at the air–aqueous solution interface, as a result of complementarity between the amphiphilic head groups and the crystal surface (4). Coupling this observation with the above reports suggested that hemozoin nucleation occurs at a lipid–water interface. On the premise that hemozoin nucleation is induced via a surface layer of lipid glycerol groups that expose OH, CH_2, and oxygen lonepairs, nucleation was predicted to occur via the {100} face, which exposes CO_2H and C—H groups (5). Precipitation of micron-sized crystals of β-hematin from a myristoyl–glycerol solution/water interface was reported by Egan et al. (6). The orientation of such crystals at the water surface was identified by grazing incidence X-ray diffraction, revealing crystals floating on their {100} faces, but not the presence of lipid layers (7). Egan and co-workers extended this work, employing fluorescence, confocal, and transmission electron microscopic imaging. They demonstrated that the β-hematin crystallized at the water interface of spherical particles with a homogeneous (i.e., "solid") core, according to confocal microscopy (8). By comparison, β-hematin, grown in an $O{=}S(CH_3)_2 : CH_3OH : CH_3Cl$ solution, in contact with a self-assembled $HS{-}(CH_2)_{11}OH$ monolayer exposing OH groups, was nucleated at the monolayer interface via its {100} face, whereas the monolayer, exposing a 1 : 1 mixture of OH and CH_3 groups, promoted nucleation equally via {100} and {010} faces (7). Similar crystallization results were obtained by Wang et al. in an acidic aqueous solution (9).

In contradistinction to the templated nucleation of β-hematin, Coppens and Vielemeyer (10) and Pisciotta et al. (11) described hemozoin crystals enveloped by neutral lipid droplets inside the DV (thus apparently formed therein), detected by use of Malachite green during chemical fixation for transmission electron microscopy. Using mass spectroscopy, Pisciotta et al. identified mainly monoacylglycerol lipids in association with isolated hemozoin. Tilley and co-workers (12), using cryo soft X-ray tomography with a 50-nm resolution, observed rod-like hemozoin crystals in the DV, and noted that lipid nanodroplets encasing hemozoin crystals may augment the X-ray absorption signal.

It is difficult to reconcile the observation of hemozoin crystals embedded within a lipid nanosphere with the concept of induced nucleation of hemozoin at a lipid surface. Templated nucleation yielding oriented hemozoin crystals, induced via acylglycerol lipids, implies aglycerol head group layer interfaced to water. To better characterize the nucleation process, we used synchrotron X-ray techniques to determine relative crystal orientation within a hemozoin cluster. The issue is further examined in a companion report (13) probing *Plasmodium*-infected RBCs by cryo soft X-ray tomography (cryo-XT) and electron microscopy.

We describe use of a noninvasive procedure capable of scanning many RBCs, singling out those that contain hemozoin crys-

Author contributions: S.K., F.P., J.A.-N., and L.L. designed research; S.K., T.B., M.D., A.M., J.A.-N., and L.L. performed research; S.K., T.B., L.H., M.D., A.M., F.P., and J.A.-N. contributed new reagents/analytic tools; S.K., J.A.-N., and L.L. analyzed data; and J.A.-N. and L.L. wrote the paper.

The authors declare no conflict of interest.

*This Direct Submission article had a prearranged editor.

Freely available online through the PNAS open access option.

[1]To whom correspondence may be addressed. E-mail: als@fys.ku.dk or leslie.leiserowitz@weizmann.ac.il.

This article contains supporting information online at www.pnas.org/lookup/suppl/doi:10.1073/pnas.1118134109/-/DCSupplemental.

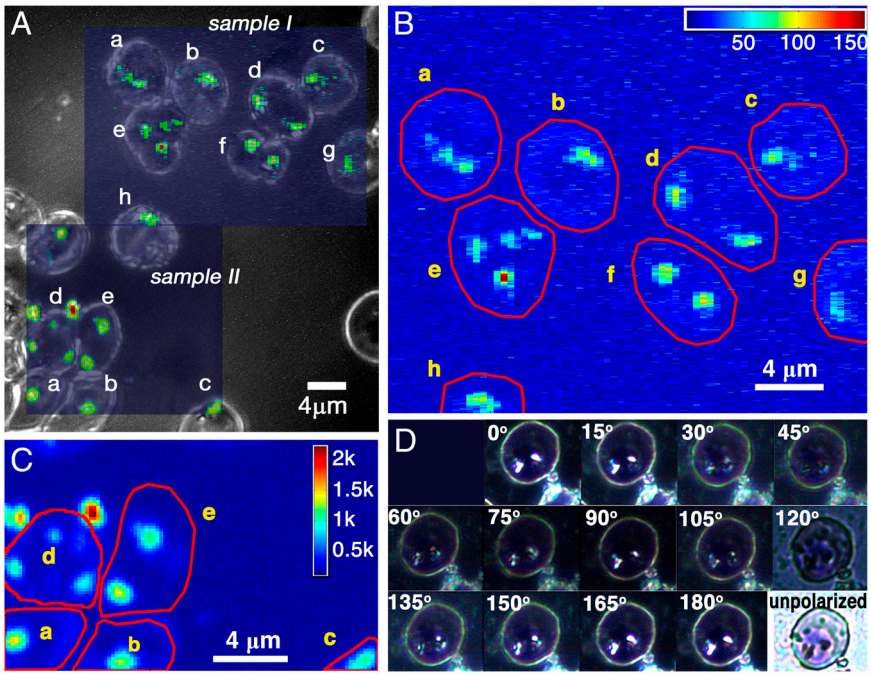

Fig. 1. (*A*) The optical micrograph of *Plasmodium*-infected RBCs onto which the X-ray Fe fluorescence patterns are superimposed. The pure optical micrograph is shown in Fig. S1. (*B* and *C*) The X-ray Fe fluorescence patterns of samples I and II. Note that the two Fe-rich particles outside cell *d* in *C* are extraneous. (*D*) Optical light birefringence pattern of an infected RBC as a function of rotation of crossed polarizers. The birefringence of hemozoin crystals in infected RBCs using crossed polarizers has already been reported by Lawrence and Olson (16).

tals for detailed examination. The method involves use of a synchrotron X-ray nanoprobe to locate the hemozoin crystals by X-ray Fe fluorescence, and to obtain concomitantly X-ray diffraction measurements therefrom. The fluorescence also yielded an estimate of the hemozoin amount in each cluster and the diffraction provided evidence of hemozoin crystal alignment therein.

Details on the preparation of the *P. falciparum*–infected RBC samples (I) and (II), their optical visualization (Fig. 1*D* and Fig. S1), and the X-ray Fe fluorescence and diffraction measurements (using X-ray beams of size 0.4×0.08 and 1×1 μm^2) (Fig. S2) are given in *Materials and Methods* and *SI Text*.

Results

The X-Ray Fe Fluorescence and Diffraction Patterns. The areas of high Fe content correspond to hemozoin clusters (Fig. 1 *B* and *C*). They matched the optical presence of the malaria pigment (Fig. 1*A*); more importantly, the X-ray diffraction signals (Fig. S3) obtained from these areas yielded *d* spacings corresponding to the most intense X-ray reflections of β-hematin (14), allowing {hkl} assignment thereto (Table 1).

By comparing the Fe fluorescence signal from the hemozoin clusters to that from a reference Fe foil, the hemozoin content in each cluster was determined, as detailed in Figs. S4 and S5 (Table 2). The low amount of hemozoin produced in RBCs *a*, *b*, *c*, *g*, and *f* (Table 2) suggests a trophozoite stage [Table S1 in the companion report (13)]; *f* is possibly a doubly invaded parasitized RBC; *e* might be either doubly invaded or composed of two partially overlapping cells according to its shape (Fig. 1*A*) in which the lower cell contains the Fe-rich particle. By asserting an average hemozoin crystal volume to be 0.0085 μm^3, as derived from Table S1 in the companion report (13), the number of crystals in each RBC (Table 2) was estimated. It is noteworthy that the volume 0.0085 μm^3 corresponds to dimensions $\approx 0.13 \times 0.13 \times 0.45$ μm^3, given that the relative dimensions of hemozoin along its *a*, *b*, and *c* axes are ≈1:1:3.5, according to its theoretical growth habit (15).

It is clear for at least two reasons that the hemozoin crystals in a cluster in the DV tend to be oriented. One is that birefringence would be washed out in a cluster of randomly oriented hemozoin crystals, which is in contradiction to the pronounced effect of crossed polarizers in the optical image in Fig. 1*D*. The other reason is based on statistical analysis of the X-ray diffraction. The probability, p_1, for occurrence of any particular single

Table 1. Summary of results from X-ray diffraction and Fe fluorescence measurements of sample I: *hkl* indices of hemozoin X-ray reflections, the number thereof, average intensity, observed *d* spacing, and corresponding *d* spacing of β-hematin

hkl	*N*r	⟨*I*⟩	*d* (obs)	*d* (BH)
1 0 0	13	127	12.05	11.99
0 2 0	2	54	7.30	7.27
1 $\bar{2}$ 0	1	77	5.87	5.87
2 $\bar{1}$ $\bar{1}$	1	43	5.00	4.98
0 3 1	4	92	4.13	4.11
1 3 1	10	68	3.71	3.69

Table 2. Summary of results from diffraction and fluorescence data, sample I: labeled RBCs, volume of hemozoin Vol(hz) (μm^3), estimated number of crystals, *Nx*, and fraction of hemoglobin, Hgb, consumed to produce hemozoin

RBC	Vol (hz)	*N*x	Hgb
a	0.112	13	0.2
b	0.099	12	0.1
c	0.091	11	0.1
d	0.175	21	0.2
e	0.228	27	0.4
f	0.191	23	0.3
g	0.064	8	0.1
h	0.117	14	0.2

Nx≈Vol/0.0085, where 0.0085 μm^3 is the average hemozoin crystal volume per infected RBC as derived from Table S1 in the companion report (13).

(*hkl*) reflection from a cluster can be estimated as the product of the number of crystals in the cluster, ≈10, and the inverse number of reflecting (*hkl*) Bragg planes in one crystal, about 100, see Fig. S6. The latter gives the extension of a Bragg point to a Bragg volume as one proceeds from a macroscopic crystal to a nanocrystal (detailed in *SI Text*). For hemozoin crystals, the order of magnitude is $p_1 \approx 0.1$. Were the crystals in the cluster randomly oriented, the probability for simultaneous observation of any particular *hkl* reflection from *n* different crystallites within that cluster would be $(p_1)^n$. Observations of five or more reflections (*vide infra*) would be vanishingly improbable.

Hemozoin Crystal Alignment Within a Cluster. We now describe models for mutual crystallite orientation within the hemozoin clusters, derived from the diffraction results. Given that the sample was not rotated, the most intense reflections—{100}, {031}, and {131}—had the highest probability of being observed, as was the case (Table 1). Thus, we confine the analysis of crystal alignment in terms of these three reflections. We focus on hemozoin clusters in RBCs *b* and *f* (sample I), and RBC *a* (sample II).

The RBC *b* contains one hemozoin cluster, which yielded five {131} Bragg peaks (2′–6′) and one {031} peak (1′), the distribution of which is depicted in Fig. 2*A*, *u*. The locus of end points of the five d^*{131} diffraction vectors (Fig. 2*A*, *l*) lie on a curved line with the same sequence of corresponding crystals on the X-ray fluorescence scan (*Inset*, Fig. 2*A*, *u*), which is consistent with hemozoin crystals arranged on a curved surface, with a common cylindrical axis.

The reflection patterns from RBCs *f* and *a* (Fig. 2 *B* and *C*) incorporate features consistent with several hemozoin crystals aligned along their needle *c* axes, oriented with their {100} faces towards a curved surface (Fig. 3). This model was deduced from the geometry of the {100} and {131} reflection pairs (6′,3′) and (4′ or 5′, 2′) from RBC *f*, and reflection pair (1′, 5′), complemented by the set of {100} reflections 2′–4′, from the RBC cluster *a*. The model diffraction correlation is explained in the caption of Fig. 3 *A* and *B*.

This model arrangement of aligned hemozoin crystals is supported by the cryo-XT image of a trophozoite DV of *P. falciparum*, presented in the companion paper (13), shown here in Fig. 3*C*. The aligned crystals lie close to the inner membrane surface of the DV, exposing their {100} faces to the membrane surface according to their morphology (15).

Summary and Conclusion. The feasibility of examining clusters of hemozoin crystals in *Plasmodium*-infected RBCs by a synchrotron X-ray nanoprobe has been demonstrated. We were able to locate the hemozoin clusters and estimate the amount of hemozoin therein. The X-ray diffraction patterns obtained from some of these clusters are interpreted in terms of hemozoin alignment, with the crystals oriented essentially parallel along their needle *c* axes, exposing their {100} faces to a curved surface. This interpretation is consistent with nucleation of hemozoin via an acyl glycerol lipid surface, but not a proof thereof, nor does it provide information on the location of such a lipid surface. Regarding the conundrum of relating templated hemozoin nucleation with the observation of hemozoin crystals enveloped within a lipid droplet (*vide supra*), it is difficult to conceive how a cluster of aligned crystals may be formed therein. Finally, although we cannot rule out that agglomeration occurred after nucleation, it does not exclude face-oriented nucleated hemozoin needles becoming aligned by contact. These intertwined questions are settled in the companion report (13).

Materials and Methods

Sample Preparation. The RBC samples were prepared by smearing magnetically concentrated *P. falciparum*–infected RBCs stained in Giemsa solution onto a 50-μm thick, 10-mm diameter glass plate. For navigation across the sample, a quadratic grid of labeled Cu bars with a square size of 63 μm

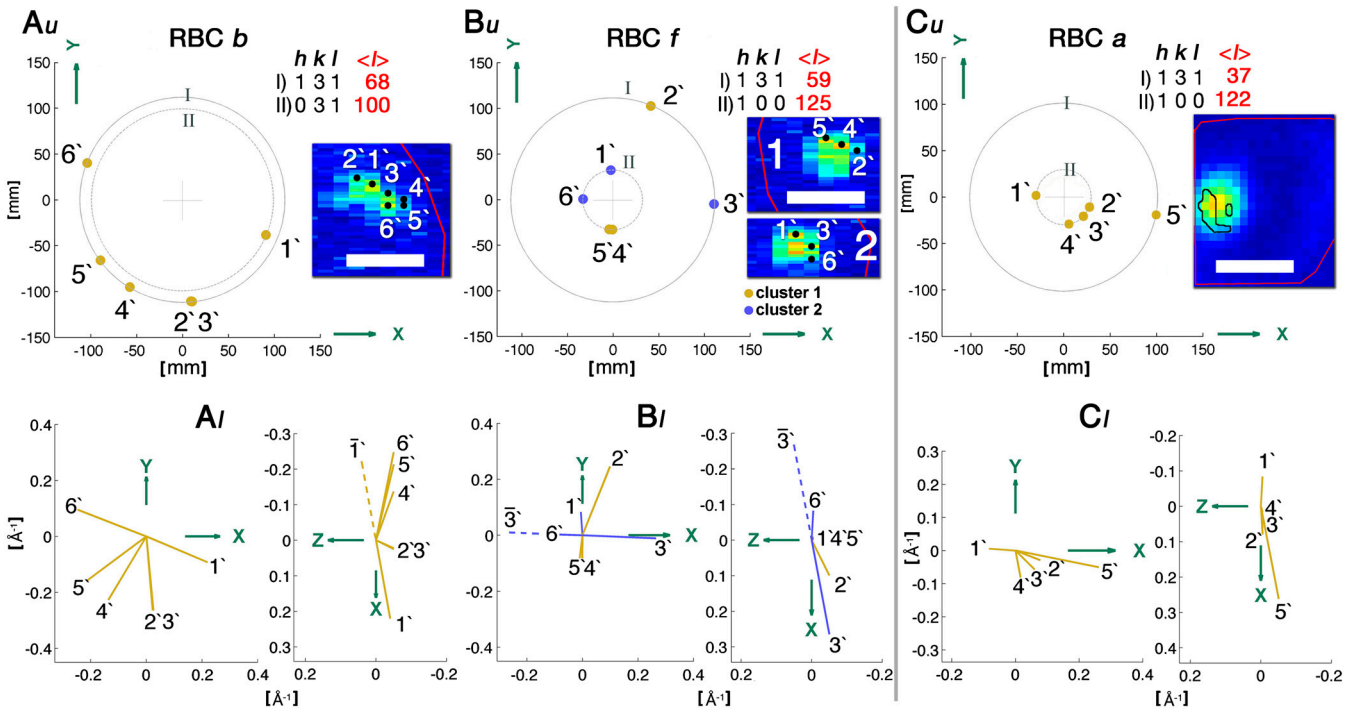

Fig. 2. (*A*, *u*; *B*, *u*; *C*, *u*) Bragg reflection positions on PILATUS (a two-dimensional X-ray detector). The X-ray diffraction patterns, in the form of Debye–Scherrer rings, arise from the hemozoin clusters in RBCs *b* and *f* of sample I, and RBC *a* of sample II. *Insets* are the corresponding X-ray Fe fluorescence patterns (Fig. 1*B* and *C*), denoting the positions at which the diffraction signals were obtained. (*A*, *l*; *B*, *l*; *C*, *l*) The diffraction vectors, d^*, with components d^*x, d^*y, and d^*z, which correspond to the Bragg peaks that appear on the PILATUS detector, as viewed along the *z* (*Left*) and *y* (*Right*) axes. (The *x*, *y*, and *z* axes are also depicted in Fig. S2.) Note that peaks 2′ and 3′ in *A* almost coincide, yet might be different reflections according to analysis (*SI Text*). Analogously, although peaks 1′ and 6′ might arise from simultaneous diffraction from the same crystal, analysis (*SI Text*) indicates two antiparallel crystals. Scale (*Insets*), 2 μm.

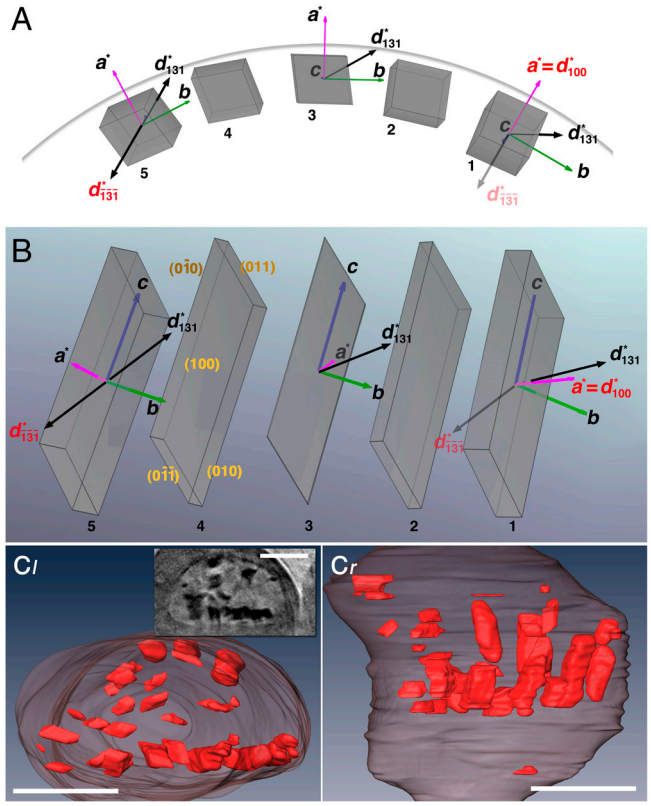

Fig. 3. Model of hemozoin crystal alignment on a curved surface. (*A*) Five rod-like crystals (labeled 1 through 5) are depicted, with their *c* axes aligned approximately parallel to the viewing direction and their {100} faces exposed to the surface of a cylinder, lying along a curved line. The crystal morphology [which is needle-like, exposing {100} and {010} side faces and (011) slanted end faces] is based on an analysis of the theoretical growth form of β-hematin and observed morphology of hemozoin (15). (*B*) View of the five crystals along the cylinder radius passing through crystal 3. The model is consistent with simultaneous diffraction of {100} and $(\bar{1}\,\bar{3}\,\bar{1})$ reflections, 1′ and 5′ in Fig. 2*C* (and with reflections 5′ and 2′, and 6′ and 3′ in Fig. 2*B*): The observed angle between diffraction vectors $d^*(100)$ of crystal 1 and $d^*(\bar{1}\,\bar{3}\,\bar{1})$ of crystal 5 is 166°, so the angle between $d^*(100)$ and $d^*(131)$ is 14°. In one and the same crystal of β-hematin, this angle is 62°. The vector and label of $d^*(\bar{1}\,\bar{3}\,\bar{1})$ attached to crystal 1 are semitransparent because they belong to crystal 5. Going from crystal 1 to 5, the crystals are rotated in steps of 14.5° about their *c* axis (a total of 58°) and 3.3° about their *b* axis, resulting in the observed angular difference of 14° between $d^*(100)$ of crystal 1 and $d^*(131)$ of crystal 5. The model is basically consistent with the observed {100} reflections 1′, 2′, 3′, and 4′ shown in Fig. 2*C*, which would require crystal rotations only about the *c* axis, and with the {100}-oriented nucleation of β-hematin induced at various interfaces (7). (*C*) View taken from report (13) of segmented cryo-XT of a trophozoite DV, displaying hemozoin crystals lining the DV's membrane, and (*Inset*) a reconstructed tomogram section viewed along the same direction. (Scale bars: 1 μm.)

was glued on the opposite side of the smear. The RBCs were visualized in an optical microscope, shown in Fig. 1 *A* and *D* and Fig. S1. Later, the same RBCs could be positioned in the X-ray beam because the labeling also appeared in the X-ray radiography of the Cu grid.

X-Ray Measurements. The experiments were conducted at the cSAXS beamline of the Swiss Light Source using a nanofocus X-ray beam setup (Fig. S2). A monochromatic X-ray beam was focused to a 400 × 80-nm^2 spot, yielding a flux of $5 \cdot 10^8$ photons/s. The first sample (I) was scanned in steps equal to the spot size over an area of 30 × 24 μm^2. At each step lasting 0.1 s, the Fe fluorescence yield was determined, and X-ray diffraction data accumulated for 0.25 s provided the Fe fluorescence signal was above noise level. For the second sample (II), the beam was focused to a 1-μm diameter and scanned over the sample area of 20 × 20 μm^2 in 0.2-μm steps.

ACKNOWLEDGMENTS. We thank M. Burghammer, H. Bruus, F. Jensen, K. Martinez, C. Riekel, and D. Sullivan for assistance in the early part of the work; I. Weissbuch and M. Elbaum for discussions; the SLS for beamtime; and O. Bunk and X. Donath for technical assistance thereat. M.D. and F.P. acknowledge support from the Deutsche Forschungsgemeinschaft Cluster of Excellence Munich-Centre for Advanced Photonics; S.K. acknowledges support from The Kimmelmann Center.

1. Goldberg DE, Slater AFG, Cerami A, Henderson GB (1990) Hemoglobin degradation in the malaria parasite *Plasmodium falciparum*: An ordered process in a unique organelle. *Proc Natl Acad Sci USA* 87:2931–2935.
2. Fitch CD, Cai GZ, Shen YF, Shoemaker DJ (1999) Involvement of lipids in ferriprotoporphyrin IX polymerization in malaria. *Biochim Biophys Acta* 1454:31–37.
3. Jackson KE, et al. (2004) Food vacuole-associated lipid bodies and heterogeneous lipid environments in the malaria parasite *Plasmodium falciparum*. *Mol Microbiol* 54:109–122.
4. Kuzmenko I, et al. (2001) Design and characterization of thin films architectures at the air-liquid interface: Simplicity to complexity. *Chem Rev* 101:1659–1696.
5. Solomonov I, et al. (2007) Crystal nucleation, growth and morphology of the synthetic malaria pigment β-hematin and the effect thereon by quinoline additives: The malaria pigment as a target of various antimalarial drugs. *J Am Chem Soc* 129:2615–2627.
6. Egan TJ, et al. (2006) Haemozoin (β-haematin) biomineralization occurs by self-assembly near the lipid/water interface. *FEBS Lett* 580:5105–5110.
7. de Villiers KA, et al. (2009) Oriented nucleation of β-hematin crystals induced at various interfaces: Relevance to hemozoin formation. *Cryst Growth Des* 9:626–632.
8. Huang AN, et al. (2010) Crystallization of synthetic haemozoin (β-haematin) nucleated at the surface of lipid particles. *Dalton Trans* 39:1235–1244.
9. Wang X, Ingall E, Lai B, Stack AG (2010) Self-assembled monolayers as templates for heme crystallization. *Cryst Growth Des* 10:798–805.
10. Coppens I, Vielemeyer O (2005) Insights into unique physiological features of neutral lipids in apicomplexa: From storage to potential mediation in parasite metabolic activities. *Int J Parasitol* 35:597–615.
11. Pisciotta JM, et al. (2007) The role of neutral lipid nanospheres in *Plasmodium falciparum* haem crystallization. *Biochem J* 402:197–204.
12. Hanssen E, et al. (2011) Cryo transmission X-ray imaging of the malaria parasite *P. falciparum*. *J Struct Biol* 173:161–168.
13. Kapishnikov S, et al. (2012) Oriented nucleation of hemozoin at the digestive vacuole membrane in *Plasmodium falciparum*. *Proc Natl Acad Sci USA* 109:11188–11193.
14. Pagola S, Stephens WP, Bohle DS, Kosar AD, Madsen SK (2000) The structure of malaria pigment (β-haematin). *Nature* 404:307–310.
15. Buller R, Peterson ML, Almarsson O, Leiserowitz L (2002) Quinoline binding site on malaria pigment crystal: Rational pathway for antimalarial drug design. *Cryst Growth Des* 2:553–562.
16. Lawrence C, Olson JA (1986) Birefringent hemozoin identifies malaria. *Am J Clin Pathol* 86:360–363.